LETTERS

In situ observation of incompressible Mott-insulating domains in ultracold atomic gases

Nathan Gemelke[1], Xibo Zhang[1], Chen-Lung Hung[1] & Cheng Chin[1]

The observation of the superfluid to Mott insulator phase transition of ultracold atoms in optical lattices[1] was an enabling discovery in experimental many-body physics, providing the first tangible example of a quantum phase transition (one that occurs even at zero temperature) in an ultracold atomic gas. For a trapped gas, the spatially varying local chemical potential gives rise to multiple quantum phases within a single sample, complicating the interpretation of bulk measurements[1–5]. Here we report spatially resolved, *in-situ* imaging of a two-dimensional ultracold atomic gas as it crosses the superfluid to Mott insulator transition, providing direct access to individual characteristics of the insulating, superfluid and normal phases. We present results for the local compressibility in all phases, observing a strong suppression in the insulator domain and suppressed density fluctuations for the Mott insulator, in accordance with the fluctuation–dissipation theorem. Furthermore, we obtain a direct measure of the finite temperature of the system. Taken together, these methods enable a complete characterization of multiple phases in a strongly correlated Bose gas, and of the interplay between quantum and thermal fluctuations in the quantum critical regime.

Since its theoretical inception[6–8], two of the most celebrated properties of the bosonic Mott insulator have been its incompressibility and suppression of local density fluctuations[9], induced by the enhanced importance of inter-particle repulsion for particles subject to a strong lattice potential. The result for a trapped atom gas is the remarkable 'wedding-cake' density profile, in which successive Mott-insulator domains appear as plateaus of constant density. Related phenomena have been studied through the coherence[1,2], transport[1,3], noise correlations[4], and number variance[5,10], but direct observation of the incompressibility has proved difficult owing to the inhomogeneous nature of all experiments to date, and to the technical difficulty of making spatially resolved measurements. Innovative experimental efforts incorporating tomographic imaging and other advanced techniques have yielded evidence[11,12] that shell structure exists in the Mott insulator regime, though no-one has directly observed the incompressibility of the insulating density plateaus by imaging a complete and single physical system *in situ*.

We report studies based on direct *in-situ* imaging of an atomic Mott insulator. By loading a degenerate Bose gas of caesium-133 atoms into a thin layer of a two-dimensional (2D) optical lattice potential, and adiabatically increasing the optical lattice depth, we observe the emergence of an extremely flat density near the centre of the cloud, which corresponds to a Mott-insulator phase with accurately one atom per site. From density profiles, we extract important thermodynamic and statistical information, confirming the incompressibility and reduction of density fluctuations in the Mott insulator as described by the fluctuation–dissipation theorem.

The single-layer 2D optical lattice is formed by two pairs of counter-propagating laser beams derived from a Yb fibre laser at wavelength $\lambda = 1{,}064$ nm. The pairs are oriented orthogonally on the horizontal (x–y) plane, forming a square lattice with site spacing $d = \lambda/2 = 0.532\,\mu$m. A weak harmonic potential of $V_h = m(\omega_x^2 x^2 + \omega_y^2 y^2)/2$ localizes the sample, where m is the caesium mass, and the geometric mean of the principal trap frequencies $\omega_{x,y}$ is $\omega_r = \sqrt{\omega_x \omega_y} = 2\pi \times 9.5$ Hz, where subscript r refers to radial direction (a weak dependence on lattice depth is described in the Methods). Vertical confinement is provided by an additional vertical optical lattice with a site spacing of 4 μm, formed by two beams intersecting at an angle of 15°, confining atoms in a Gaussian wavepacket of width (oscillator length) $a_z = 0.30\,\mu$m. The sample is loaded into a single site of the vertical lattice, kept deep to prevent vertical tunnelling. Tunnelling in the horizontal 2D lattice is controlled by varying the lattice depth V (ref. 1). Details on preparation of the atomic sample can be found in the Supplementary Information and ref. 13.

We obtain a top view of the sample using absorption imaging, directly revealing the atomic surface density $n(x, y)$ on the horizontal plane. The imaging resolution is 3–4 μm, and magnification such that one imaging pixel corresponds to an area of $(2\,\mu\text{m})^2$ on the object plane. Unit filling in a 2D optical lattice has a conveniently measurable optical absorption on resonance.

The superfluid to Mott insulator transition of ultracold atoms in an optical lattice is described by the Bose–Hubbard model, characterized by

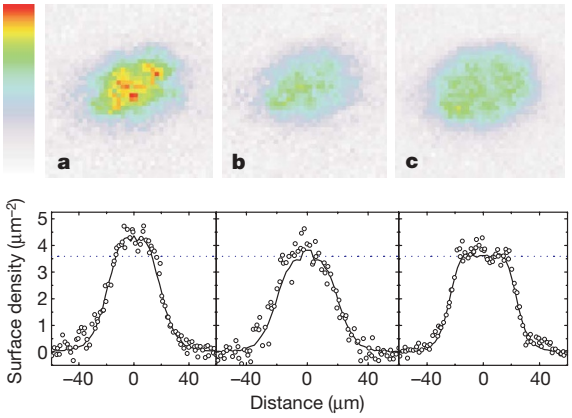

Figure 1 | False-colour absorption images and line cuts along major axis of density profiles for $N = 7{,}500$ ultracold caesium atoms at scattering length $a = 310a_B$ in 2D optical lattices. a, Superfluid regime (shallow lattice $V = 2.4E_R$); **b**, phase transition regime (medium lattice depth $V = 9.4E_R$); and **c**, Mott-insulator regime (deep lattice $V = 22E_R$). Images are averaged over three experiment repetitions. The colour scale shows linear variation with density from zero to the peak value of 5.4 μm^{-2}. Line cuts are taken along the major axis, and compared to radial average of density (solid line) over the entire image as described in text. The blue horizontal dotted line indicates the density of one atom per site.

[1]The James Franck Institute and Department of Physics, University of Chicago, Chicago, Illinois 60637, USA.

on-site interaction U and the tunnelling strength J (ref. 8). In 2D optical lattices, superfluid is converted into a Mott insulator when U/J exceeds 16 near the density of one atom per site[2,14]. Here, the superfluid–Mott insulator phase transition can be induced by either increasing the lattice potential depth V (typically measured in units of recoil energy $E_R = h \times 1.3$ kHz, where h is Planck's constant)[1,2,12] or the atomic interaction strength (characterized by scattering length a, typically measured in Bohr radii a_B) via a magnetically tuned Feshbach resonance[15], together providing complete, independent control of U and J.

Atomic density profiles in the lattice are shown in Fig. 1. For weak lattice depths (superfluid regime), the density profiles are bell-shaped, with negative curvature at the centre (Fig. 1a), indicating a finite, positive compressibility dictated by the interaction coupling constant (discussed below). In sufficiently deep lattices, we observe a flattened density at the centre of the sample (Fig. 1b, c), indicating development of a Mott-insulating phase with one particle per lattice site. This density plateau, an important feature of the Mott-insulator phase, arises from incompressibility.

A primary check on the Mott insulator is to compare the measured density in the plateau to that corresponding to one atom per site, given by Mott-insulator physics as a 'standard candle' of atomic density. Using the known scattering cross-section, correcting for saturation effects (see Methods), we determine the plateau density (and standard error, in parentheses) to be $n = 3.5(3)\ \mu m^{-2}$, in agreement with the expected value $1/d^2 = 3.53\ \mu m^{-2}$.

To distinguish a Mott insulator from superfluid or normal gas, we histogram the occurrence of pixels $h(n)$ in the images corresponding to a density n within a small bin size Δn. The Mott-insulator plateau, containing a large number of pixels with similar atomic density, appears as a peak at $n = 1/d^2$ (Fig. 2a). In general, the occurrence of a particular density n can be regarded as the rate at which local chemical potential changes with density, multiplied by the number of pixels $w(\mu)\Delta\mu$ corresponding to a chemical potential between μ and $\mu + \Delta\mu$. The occurrence at density n is then $h(n) = \Delta n\omega(\mu)\Delta\mu/\Delta n \approx \Delta n\omega(\mu)\kappa^{-1}$, where $\kappa = \partial n/\partial\mu$ is the local compressibility[16]. In a harmonic trap, $\omega(\mu) = 2\pi/md^2\omega_r^2$ is constant, and the histogram is a particularly useful tool for distinguishing different phases. For a pure Bose–Einstein condensate (BEC) in the Thomas–Fermi limit, the compressibility is constant up to the peak density n_{peak}, and results in a constant $h(n)$ for $n \le n_{peak}$ (see Fig. 2b for $0.5/d^2 < n < 1.5/d^2$). For the Mott insulator, the density is insensitive to chemical potential in a narrow range near $n = 1/d^2$, indicating a vanishing compressibility, and thus a sharp histogram peak at $n = 1/d^2$. The peak's presence in Fig. 2a is thus directly related to the incompressibility in the Mott phase. Finally, the compressibility of a normal (ideal) gas is proportional to its density, so $h(n) \propto 1/n$, leading to the strong upturn at low densities in Fig. 2a, b for both regimes.

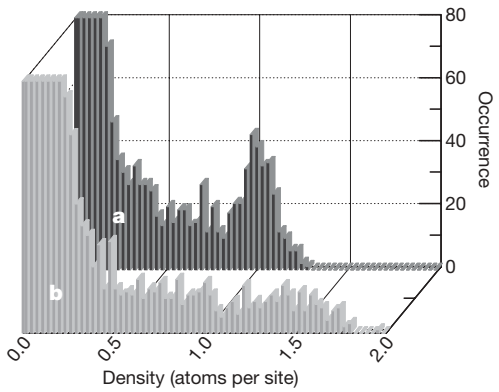

Figure 2 | Histograms of density profiles in the Mott-insulator regime and the superfluid regime. **a**, Mott-insulator regime: $V = 38E_R$, $a = 460a_B$. **b**, Superfluid regime: $V = 0.5E_R$, $a = 460a_B$. The histograms are based on an average of three density images. The bin size is $\Delta n = 0.03$. Occurrence is the number of samples (pixels) measured as a density between n and $n + \Delta n$.

Much more information can be obtained from the density profiles, as recently suggested in ref. 17. For example, the compressibility in a 2D cylindrically symmetric trap can be written $\kappa = \partial n/\partial\mu = -n'(r)/(rm\omega_r^2)$, where we have assumed the local density approximation, and that the chemical potential depends on the trapping potential $\mu = \mu_0 - V_h(r)$. For a BEC in the Thomas–Fermi regime, the compressibility is positive and constant, $\kappa_{BEC} = 1/g$, where $g = \sqrt{8\pi}a\hbar^2/ma_z$ is the 2D interaction parameter[18]. We can thereby relate the measured compressibility to that of a BEC as:

$$\frac{\kappa}{\kappa_{BEC}} = -\left(\frac{2}{\pi}\right)^{7/2}\frac{n'(r)}{rd^{-4}}\frac{a}{a_z}\left(\frac{E_R}{\hbar\omega_r}\right)^2 \qquad (1)$$

We evaluate κ from azimuthally averaged density profiles (Fig. 3a). The eccentricity of the trap is corrected by rescaling the principal axes as determined from the density profile, and verified to be consistent with direct measurement of trap frequencies. Owing to the singular nature of $n'(r)/r$ near the centre, we evaluate κ there by fitting $n(r)$ to a quadratic, $n(r) = n(0) - \alpha r^2$. The curvature α then gives the compressibility as $\kappa(0) = 2\alpha/m\omega_r^2$, for which we obtain $\kappa/\kappa_{BEC} = 0.34(10)$ in a weak lattice and $\kappa/\kappa_{BEC} = 0.013(6)$ in a strong lattice (see Fig. 3). In the weak lattice (superfluid regime), the finite and constant compressibility at the centre agrees with expectation for the superfluid phase, though lower than expected, which we attribute to finite temperature and calibration of trap parameters. The finite temperature is also clear

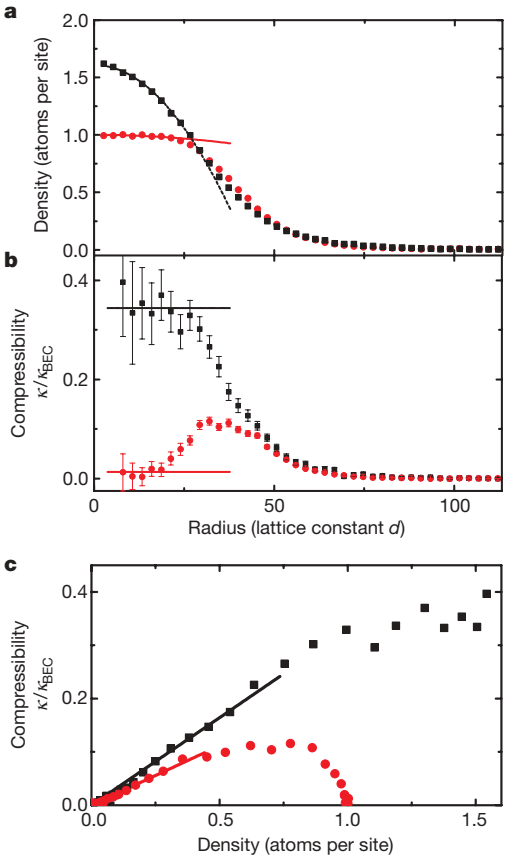

Figure 3 | Extraction of compressibility from density profiles. **a**, Radially averaged profiles (three images) in the superfluid (black squares, $V = 0.3E_R$, $N = 7{,}200$) and Mott insulator (red circles, $V = 22E_R$, $N = 6{,}700$), with $a = 310a_B$. A quadratic fit to the sample's centre extracts the curvature near $r = 0$. **b**, Normalized compressibilities derived from **a** using equation (1) in the superfluid (black squares) and Mott-insulator (red circles) regimes. The horizontal lines indicate compressibility near $r = 0$, estimated from the quadratic fits in **a**. Rising compressibility at $r = 20d$ marks the Mott-insulator boundary. **c**, The dependence of compressibility on atomic density. Linear dependence at low densities (normal gas) is best-fitted by solid lines. Error bars indicate standard error in the mean.

in the exponential tail of the density profile and the compressibility[19], from which we derive the temperature 10(2) nK in the superfluid regime ($V = 0.3E_R$) and 15(3) nK in the Mott-insulator regime ($V = 22E_R$).

In a deep lattice (Mott-insulator regime), we observe a strong reduction of the compressibility in the trap centre, below that in the superfluid phase for the weak lattice, strongly supporting the emergence of a Mott-insulator phase at the centre of the sample. Away from the centre, κ suddenly increases at $r = 20d$, then decreases for $r > 40d$. The exponential decay is again consistent with a normal gas. Between a Mott insulator and a normal gas ($20d < r < 40d$), a more detailed measurement and model of compressibility would be necessary to identify the local phase.

Within the local density approximation, one may consider any small area of the sample as a thermodynamic subsystem in a grand-canonical ensemble, assumed to be in equilibrium with the remainder of the gas. One can then invoke the fluctuation–dissipation theorem (see for example, refs 16 and 20) to ascertain that incompressibility necessarily implies a low local particle number fluctuation; this relationship takes the form:

$$\delta n^2 \approx \kappa k_B T \quad (2)$$

Resolved *in-situ* imaging provides an enticing opportunity to measure fluctuations of the local density[9,21], and thus check the validity of the fluctuation–dissipation theorem. We measured fluctuations by recording multiple absorption images, calculating the variance of density measured in each pixel (each collects signals from a patch of $(2\,\mu m/d)^2 \approx 14$ lattice sites). Figure 4 shows the recorded fluctuations, where pixels are binned according to their mean atomic density. Fluctuations consist of detection (photo-electron shot) noise and thermal and quantum atomic density fluctuations. Detection shot noise can be well-calibrated and modelled by analysing portions of the images with low density; extension to higher optical depth (density) shows the weak dependence illustrated in Fig. 4.

Above the detection noise, density fluctuations (see Fig. 4) show a strong qualitative agreement with the compressibility presented in Fig. 3, as expected from the fluctuation–dissipation theorem. For example, the Mott-insulator phase shows a strong suppression of fluctuations at the density of one atom per site. The superfluid regime lacks this feature, instead showing a pronounced flattening as the sample transitions from normal gas to superfluid, as expected from the constant compressibility in the superfluid phase (Fig. 3c). Finally, at low density, the normal gas shows a temperature-independent fluctuation of $\delta n = \gamma\sqrt{n}$, which can be anticipated from Fig. 3c, and agrees with the fluctuation–dissipation theorem. The coefficient γ is roughly consistent with the fluctuation–dissipation theorem, and the measured imaging resolution (see Methods).

Clearly, *in-situ* imaging of the Mott insulator is a powerful new tool with which to investigate new quantum phases of cold atoms in optical lattices. From the density profiles, not only can we observe the density plateau, incompressibility and reduction of fluctuations in the Mott insulating phase, but also demonstrate a qualitative validation of the fluctuation–dissipation theorem. Relatively modest extension of this work holds new promise for studying the role of quantum fluctuations, correlation and thermodynamics near a quantum phase transition.

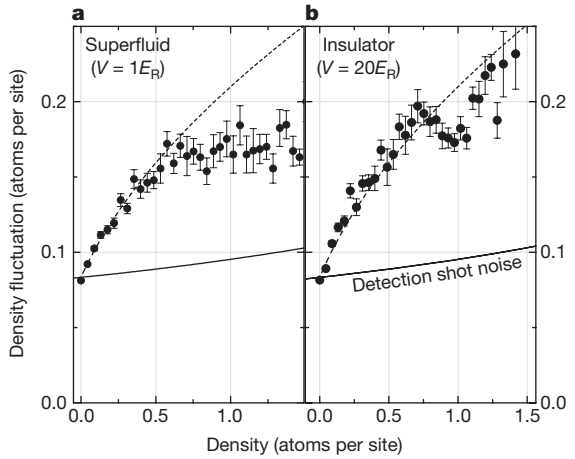

Figure 4 | The fluctuation of local density extracted from a set of eleven absorption images in the weak and deep lattice regimes. The insulator and superfluid show a pronounced difference at one atom per site, where the insulator's fluctuation is suppressed by incompressibility. In the superfluid, constant compressibility initiates a flattening. At low densities, in both the weak (**a**) and the deep (**b**) lattice regimes, the fluctuation shows a characteristic $\sqrt{n}$ dependence, where the gas is presumed to be normal; the dashed line shows the best-fitted $\sqrt{n}$ dependence. The total number of atoms was $N = 8{,}300$ (superfluid) and $N = 9{,}600$ (Mott insulator) with $a = 310a_B$ for both sets. Error bars indicate standard error in the mean.

METHODS SUMMARY

Caesium Bose condensates are produced by forced evaporative cooling in a crossed-beam dipole trap. The condensate is compressed vertically by loading into a single layer of an optical lattice with the scattering length tuned near zero. After this, the lattice is adiabatically applied by controlled retroreflection of dipole trapping beams, and the scattering length brought to its final value. Imaging is performed absorptively along the vertical, calibrated for saturation effects by varying the intensity of the imaging light. Fluctuations of density are calculated for each pixel in a series of images taken at identical experimental parameters, and plotted against the mean density at that pixel. The parameter γ is estimated from a model of the expected averaging of thermal fluctuations over an imaging resolution limited spot. Further details may be found in the online-only Methods and in the Supplementary figure.

Full Methods and any associated references are available in the online version of the paper at www.nature.com/nature.

Received 2 May; accepted 25 June 2009.

1. Greiner, M., Mandel, O., Esslinger, T., Hansch, T. W. & Bloch, I. Quantum phase transition from a superfluid to a Mott insulator in a gas of ultracold atoms. *Nature* **415,** 39–44 (2002).
2. Spielman, I. B., Phillips, W. D. & Porto, J. V. Condensate fraction in a 2D Bose gas measured across the Mott-insulator transition. *Phys. Rev. Lett.* **100,** 120402 (2008).
3. Kohl, M., Moritz, H., Stoferle, T., Schori, C. & Esslinger, T. Superfluid to Mott insulator transition in one, two and three dimensions. *J. Low-Temp. Phys.* **138,** 635–644 (2005).
4. Folling, S. *et al.* Spatial quantum noise interferometry in expanding ultracold atom clouds. *Nature* **434,** 481–484 (2005).
5. Gerbier, F., Folling, S., Widera, A., Mandel, O. & Bloch, I. Probing number squeezing of ultracold atoms across the superfluid-Mott insulator transition. *Phys. Rev. Lett.* **96,** 090401 (2006).
6. Kaganov, M. I. & Chubukov, A. V. Interacting magnons. *Uspekhi Fizicheskikh Nauk.* **153,** 537–578 (1987).
7. Fisher, M. P. A., Weichman, P. B., Grinstein, G. & Fisher, D. S. Boson localization and the superfluid-insulator transition. *Phys. Rev. B* **40,** 546–570 (1989).
8. Jaksch, D., Bruder, C., Cirac, J. I., Gardiner, C. W. & Zoller, P. Cold bosonic atoms in optical lattices. *Phys. Rev. Lett.* **81,** 3108–3111 (1998).
9. Capogrosso-Sansone, B., Prokof'ev, N. V. & Svistunov, B. V. Phase diagram and thermody-namics of the three-dimensional Bose-Hubbard model. *Phys. Rev. B* **75,** 134302 (2007).
10. Greiner, M., Mandel, O., Hansch, T. W. & Bloch, I. Collapse and revival of the matter wave field of a Bose-Einstein condensate. *Nature* **419,** 51–54 (2002).
11. Folling, S., Widera, A., Muller, T., Gerbier, F. & Bloch, I. Formation of spatial shell structure in the superfluid to Mott insulator transition. *Phys. Rev. Lett.* **97,** 060403 (2006).
12. Campbell, G. K. *et al.* Imaging the Mott insulator shells by using atomic clock shifts. *Science* **313,** 649–652 (2006).
13. Hung, C. L., Zhang, X., Gemelke, N. & Chin, C. Accelerating evaporative cooling of atoms into Bose-Einstein condensation in optical traps. *Phys. Rev. A* **78,** 011604 (2008).
14. Spielman, I. B., Phillips, W. D. & Porto, J. V. Mott-insulator transition in a two-dimensional atomic Bose gas. *Phys. Rev. Lett.* **98,** 080404 (2007).
15. Chin, C., Grimm, R., Julienne, P. & Tiesinga, E. Feshbach resonances in ultracold gases. Preprint at ⟨http://arxiv.org/abs/0812.1496⟩ (2008).
16. Batrouni, G. G. *et al.* Mott domains of bosons confined on optical lattices. *Phys. Rev. Lett.* **89,** 117203 (2002).
17. Ho, T. -L. & Zhou, Q. Obtaining phase diagram and thermodynamic quantities of bulk systems from the densities of trapped gases. Preprint at ⟨http://arxiv.org/abs/0901.0018⟩ (2008).

18. Tanatar, B., Minguzzi, A., Vignolo, P. & Tosi, M. P. Density profile of a Bose-Einstein condensate inside a pancake-shaped trap: observational consequences of the dimensional cross-over in the scattering properties. *Phys. Lett. A* **302,** 131–136 (2002).
19. Gerbier, F. Boson Mott insulators at finite temperatures. *Phys. Rev. Lett.* **99,** 120405 (2007).
20. Huang, K. *Statistical Mechanics* 152–154 (Wiley, 1963).
21. Esteve, J. *et al.* Observations of density fluctuations in an elongated Bose gas: ideal gas and quasicondensate regimes. *Phys. Rev. Lett.* **96,** 090401 (2006).

Supplementary Information is linked to the online version of the paper at www.nature.com/nature.

Acknowledgements We thank T. L. Ho, R. Scalettar, E. Mueller and R. Hulet for discussions. This work was supported by NSF (grant numbers PHY-0747907, NSF-MRSEC DMR-0213745) and ARO (grant number W911NF0710576) with funds from the DARPA OLE programme. N.G. acknowledges support from the Grainger Foundation.

Author Contributions All authors contributed to the analysis and writing of this manuscript; construction of the apparatus and acquisition of data was primarily the responsibility of C-L.H. and X.Z.

Author Information Reprints and permissions information is available at www.nature.com/reprints. Correspondence and requests for materials should be addressed to C.C. (cchin@uchicago.edu).

METHODS

Preparation of BEC in a thin 2D optical lattice. The ^{133}Cs BEC is formed in a crossed-beam dipole trap by an efficient evaporative cooling method[13]. The dipole trap consists of three beams on the horizontal plane (see Supplementary figure): two orthogonal beams at the wavelength of 1,064 nm (Yb fibre laser, YLR-20-1064-LP-SF, IPG Photonics), focused to $1/e^2$ radii of 350 μm, and one CO_2 laser beam (not shown in the Supplementary figure) at the wavelength of 10.6 μm (Gem-Select 100, Coherent), focused to a vertical $1/e^2$ radius of 70 μm and horizontal radius of 2 mm. The CO_2 beam intersects the Yb fibre laser beams at an angle of 45° and provides an enhanced vertical confinement to support the atoms against gravity. With $N = 10^4$ atoms in a pure condensate, the Thomas–Fermi radii of the condensate are $(r_x, r_y, r_z) = (23, 14, 3.6)$ μm.

After a pure BEC is obtained, the sample is compressed vertically by introducing a vertical lattice, formed by two laser beams (Mephisto, Innolight) inclined at +7.5° and −7.5° relative to the horizontal plane. The vertical lattice has a spacing of 4 μm and, together with the crossed dipole trap, forms an array of 2D oblate 'pancake' potentials, with harmonic confinement frequencies of 850 Hz at its maximum depth.

To load the condensate into a single pancake trap, we first ramp the magnetic field to 17.2 G in 400 ms, reducing the s-wave scattering length to $a < 10a_B$, and then turn on the vertical lattice in 100 ms. Atomic population in other lattice sites, if any, can be identified by observing an interference pattern in time-of-flight images taken from the side. For this work, we observe a sufficiently weak interference pattern contrast, and hence conclude that over 98% of the atoms are in a single pancake trap. After the vertical lattice is fully turned on, the CO_2 laser intensity is ramped to zero in 100 ms while the scattering length is ramped to its final value by tuning the external magnetic field.

The 2D lattice potential in the horizontal (x- and y-) directions is formed by introducing retro-reflections of the 1,064 nm dipole trap beams. A continuous evolution from a pure dipole trap (with zero retro-reflection) to a 2D optical lattice (with significant retro-reflection) is achieved by passing each dipole trap beam (after it passes through the atomic cloud once) through two acousto-optic modulators controlled by the same radio-frequency source, then off a retroreflection mirror. The acousto-optic modulators induce an overall zero-frequency shift, but permit a dynamic control of the retroreflection intensity over six orders of magnitude. To load the lattice to a depth of $38E_r$, the retroreflection intensities are slowly ramped over 200 ms with an exponential waveform of 36 ms time constant. For smaller final lattice depths, the ramp waveform is fixed but duration shortened. Onsite interaction energy U and tunnelling rate J are evaluated from the measurements of the lattice vibration frequencies and band structure calculation. Envelope trapping frequencies were separately measured by exciting centre-of-mass oscillations, and found to be consistent with orientation and ellipticity of *in-situ* images of atomic density. A weak variation of the mean envelope frequency with lattice depth was measured and accounted for by the expression: $\omega_r = \sqrt{\omega_x \omega_y} = 2\pi \times 9.5(1 + V/82E_R)$ Hz.

Calibration of atomic surface density. By varying the intensity of the imaging beam, we measure the optical depth on resonance in the density plateau using $OD = \ln(M_0/M)$, where M is the number of photons collected by a charge-coupled device (CCD) pixel in the presence of the atoms and M_0 is that without the atoms. The optical depth in the plateau is extracted from a fit to the peak in the histogram. We then assume $OD = n\sigma/(1 + M_0/M_{sat})$ and fit the variation of peak optical depth to determine the optical depth in the zero intensity limit $M_0 \to 0$, and thus the surface density of the sample. Here, $\sigma = 0.347\,\mu m^2$ is the known caesium-atom optical cross-section and the fit parameter M_{sat} represents the photon number on a CCD pixel at the atomic saturation intensity.

Fluctuation of atomic density. The fluctuations in the absorption images are estimated by taking the average of 11 images under the same experimental procedure, and calculating the mean and variance of optical depth measured at each CCD pixel. Fluctuations are presumed to arise from optical shot noise, thermal atomic fluctuation, and long-lengthscale variations arising from total atom number fluctuation. The optical shot noise is calibrated by examining regions with negligible atomic density, and extended to higher optical depth using $\delta OD_{optical\ shot} \propto \sqrt{1 + e^{OD}}$. For the thermal cloud, with density $n < 0.3$ atoms per site, the fluctuation–dissipation theorem predicts $\delta N_a = \sqrt{N_a}$, with N_a the number of atoms measured in a given region. This result should be valid for a region significantly larger than the correlation length, which we expect for the normal gas to be of the order of the de Broglie thermal wavelength, expected to be less than 1.5 μm for our sample. Although each imaging pixel corresponds to an area in the object plane consisting of ~14 sites, imperfect imaging resolution is expected to effectively average away a certain fraction of the total fluctuation. This effect can be calculated, assuming statistical independence for each site, by summing the weight $w_{i,j}$ of a resolution-limited spot falling within a given pixel j for each lattice site i, giving a variance reduced by $\sum_i w_{i,j}^2$. The result for our parameters is a reduction to $\delta n = \gamma\sqrt{n}$, with $\gamma \approx 0.11(1)$. This should be compared with the fraction of the total fluctuation shown in Fig. 4 corresponding to thermal fluctuations in the superfluid regime. To make this comparison, we reject global fluctuations associated with variation of the total atom number by subtracting the variance we calculate after first applying a resolution-spoiling Gaussian blur to the images from the variance without modification. We find, for the remaining high-spatial-frequency fluctuations, a best fit to γ of 0.15(2), using a Gaussian blur $1/e^2$ radius of $r_b = 14$ μm to remove global variations (the result varies within stated error for blur radii $7\,\mu m < r_b < 28\,\mu m$). The remaining discrepancy is probably due to calibration of imaging resolution, and possibly the effect of a non-negligible correlation length.